How Volcanic Aerosols Globally Inhibit Precipitation

Zachary McGraw[1,2*] and Lorenzo M. Polvani[1,3,4]

1 Department of Applied Physics and Applied Mathematics, Columbia University, New York, NY, USA
2 NASA Goddard Institute for Space Studies, New York, NY, USA
3 Department of Earth and Environmental Sciences, Columbia University, New York, NY, USA
4 Lamont-Doherty Earth Observatory, Columbia University, Palisades, NY, USA

Abstract

Volcanic aerosols reduce global mean precipitation in the years after major eruptions, yet the mechanisms that produce this response have not been rigorously identified. Volcanic aerosols alter the atmosphere's energy balance, with precipitation changes being one pathway by which the atmosphere acts to return towards equilibrium. By assessing the atmosphere's energy budget in climate model simulations, we here show that global precipitation reduction is largely a consequence of Earth's surface cooling in response to volcanic aerosols reflecting incoming sunlight. In addition, these aerosols also directly add energy to the atmosphere by absorbing outgoing longwave radiation, and this is a major cause of precipitation decline in the first post-eruption year. We also identify mechanisms that oppose the post-eruption precipitation decline, and provide evidence that our results are robust across climate models.

Plain Language Summary

Large volcanic eruptions can emit gas into the stratosphere that chemically forms sulfate aerosol particles. These aerosols persist in the stratosphere for up to two years, and have been linked to widespread precipitation changes in studies based on observations and models. Here we identify the mechanisms through which volcanic aerosols cause their clearest precipitation impact, a temporary reduction in global mean precipitation. Volcanic aerosols globally inhibit precipitation as a result of their abilities to both reflect incoming solar radiation and absorb longwave (terrestrial) radiation. The first is the more important influence on global precipitation, which is reduced for several years as an energetic response to cooler tropospheric temperatures. Absorption of longwave radiation further reduces precipitation during the first post-eruption year, as a response to the increased energy brought into the stratosphere.

Key Points

- We identify the mechanisms of volcanic aerosol influence on global precipitation by assessing the atmospheric energy budget in simulations.
- Post-eruption precipitation reduction is mostly a consequence of a cooler surface, with latent heat balancing a less emissive troposphere.
- Volcanic aerosols also directly add energy into the atmosphere by absorbing longwave radiation, causing further precipitation reduction.

1. Introduction

Stratospheric aerosols from volcanic eruptions have been linked to multiple global disruptions in precipitation observed during the 20th century, mostly notably a decline in global mean precipitation following the 1991 eruption of Mt. Pinatubo (Adler et al., 2018; Gillett et al., 2004). The global impacts of volcanic eruptions are important to evaluate given potential impacts on societies and ecosystems, as well as implications for stratospheric aerosol geoengineering (Proctor et al., 2018; Trenberth & Dai, 2007). While climate models have substantiated that volcanic aerosols reduce global mean precipitation in the years following eruptions (Iles & Hegerl, 2014; Robock & Liu, 1994), little has been done to understand the underlying mechanisms. In this study we identify how precipitation is reduced as a consequence of volcanic aerosol presence in the stratosphere.

The atmospheric energy budget is essential for elucidating the mechanisms by which volcanic aerosols alter precipitation, as precipitation reflects the amount of latent heat cycled into the atmosphere through condensation. A perturbation to the climate system typically initiates a multitude of changes to the atmosphere's energy budget, including radiative, sensible, and latent energy responses. The atmospheric energy budget then tends toward a new equilibrium, with the sum of all energy flux changes close to zero. The precipitation response may be represented as equal to the sum of balancing terms (O'Gorman et al., 2012):

$$L\Delta P \approx \underbrace{-\Delta R_{ATM} - \Delta SH}_{\Delta Q} - \Delta H \qquad \text{Eqn. 1}$$

Here ΔP is the precipitation anomaly and L is the latent heat of condensation constant. The atmospheric radiative flux anomaly $\Delta R_{ATM} = \Delta R_{TOA} - \Delta R_{SFC}$, is the difference in radiative flux anomalies between the top-of-atmosphere and surface, and ΔSH is surface-to-atmosphere sensible heat flux anomaly. ΔR_{ATM} includes the immediate influence of aerosol-radiation interactions on the net energy flux into the atmosphere (hereafter $\Delta R_{ATM,IRF}$, where IRF is instantaneous radiative forcing, or *aerosol forcing* for short), plus radiative flux responses as the Earth-climate system adjusts to the aerosol presence. ΔH is horizontal transport of dry static energy, which includes circulation responses. ΔH can be neglected at length scales of at least several thousand kilometers (Dagan & Stier, 2020; O'Gorman et al., 2012), and since global mean precipitation is our focus we do so in most of this study. We represent the equality in Eqn. 1 as approximate (≈) because the atmosphere takes time to fully adjust to the stratospheric aerosol layer, which continuously evolves. To simplify part of our analysis, we define $\Delta Q = -\Delta R_{ATM} - \Delta SH$, the diabatic cooling excluding latent heat (or *diabatic cooling* for short), as in O'Gorman et al. (2012).

Atmospheric energy responses to a given forcing (e.g. greenhouse gases or volcanic aerosols) are most often decomposed into *rapid adjustments* (RA) and sea surface temperature (SST) mediated responses. The rapid adjustments are atmospheric energy changes other than the IRF that would occur without SSTs responding to the forcing. The *SST-mediated responses* are usually discussed

as *climate feedbacks* (in the context of climate sensitivity), but are in our case calculated in the atmospheric energy budget rather than top-of-atmosphere budget, and applied to precipitation rather than temperature changes. Correspondingly, the precipitation response ΔP can be decomposed into a fast component (ΔP_{RA}) associated with the RA, and a slow component (ΔP_{SST}) associated the longer time scales of post-eruption SST cooling. For the latent heat responses, ΔP_{RA} is commonly referred to as the precipitation *fast response* while ΔP_{SST} is the precipitation *slow response*, with these terms conveying the longer timescales of sea surface temperature adjustment than timescales for the atmosphere and land alone (Andrews et al., 2010; Samset et al., 2016).

With this decomposition, the ΔR_{ATM} term in Eqn. 1 breaks down into the aerosol forcing, $\Delta R_{ATM,IRF}$, plus the radiative responses $\Delta R_{ATM,RA}$ and $\Delta R_{ATM,SST}$. We also combine radiative and sensible heat flux terms into a diabatic cooling rapid adjustment and diabatic cooling SST-mediated response, ΔQ_{RA} and ΔQ_{SST}. Decomposing Eqn. 1 in this way yields:

$$\underbrace{L\Delta P_{RA} + L\Delta P_{SST}}_{L\Delta P} \approx \underbrace{-\Delta R_{ATM,IRF}}_{forcing \times -1} \underbrace{- (\Delta R_{ATM,RA} + \Delta SH_{RA})}_{+\Delta Q_{RA}} \underbrace{- (\Delta R_{ATM,SST} + \Delta SH_{SST})}_{+\Delta Q_{SST}} \qquad \text{Eqn. 2}$$

In our post-eruption case, precipitation does not simply balance the initial aerosol-radiation interactions ($\Delta R_{ATM,IRF}$) on its own, since precipitation in the troposphere cannot respond to stratospheric aerosols as readily as other components of the atmosphere's energy budget within ΔQ_{RA} and ΔQ_{SST}. As we will show, some terms in Eqn. 2 oppose the initial forcing while others add to it, with precipitation anomalies being one among several covarying responses. To first order, we can interpret the precipitation response as balancing the remainder between the aerosol forcing and faster-acting radiative and sensible heat responses.

By quantifying the various terms in Eqn. 2, we here identify the key mechanisms that result in post-eruption precipitation reduction. While similar analyses of the atmospheric energy budget have been performed for anthropogenic tropospheric aerosol and greenhouse gas impacts (Andrews et al., 2010; Previdi, 2010; Samset et al., 2016), they have not to the best of our knowledge been carried out for volcanic aerosols.

2. Methods

2.1. GISS ModelE2.2 simulations

The main set of simulations we examine here were produced by DallaSanta & Polvani (2022), who used the Goddard Institute for Space Studies (GISS) ModelE2.2. ModelE2.2 is a "high-top" version of the NASA GISS ModelE Earth system model created to optimize stratospheric climate (Orbe et al., 2020), with 102 vertical levels in total and a model top at 0.002 hPa. Among several tropical eruption cases generated therein, we analyze the simulations of a 20 Tg sulfur (S)

injection case. This represents a sulfur injection between the magnitudes of Mt. Pinatubo's 1991 eruption and the larger 1815 eruption of Mt. Tambora. We chose this relatively large eruption magnitude to provide enough signal to dominate over precipitation's internal variability on a global scale.

We analyze two 20-member ensembles of ModelE2.2 runs: one ensemble with a fully coupled model configuration, where SSTs are capable of responding to the eruption, and the other with a land-atmosphere only configuration and prescribed SSTs unable to respond. We refer to these ensembles as *interactive SST* and *fixed SST* cases, respectively. For both ensembles, each member is branched off from a separate ENSO-neutral state of a long control run having pre-industrial forcings, with a tropical eruption occurring on the following June 15th. Volcanic aerosols are input as aerosol extinction and size values created with the Easy Volcanic Aerosol forcing generator (Toohey et al., 2016). In the fixed SST runs, the SSTs are taken from the corresponding years of the control run, wherein no eruption occurs. Subtracting values from the two ensembles, pairwise, isolates the role of SST-mediated responses (only present with interactive SSTs) from the direct aerosol forcing and rapid adjustments. Subtracting values from the corresponding control runs defines the post-eruption response in each case, also referred to as the post-eruption anomaly. We also assess the spread across each 20-member ensemble to quantify the magnitude of internal variability. Volcanic aerosol radiative forcings (the IRF) are calculated online at each time step, by the model itself using double radiation calls with and without factoring in the volcanic aerosols. For the atmospheric aerosol radiative forcings used in our analysis, we use the difference between top-of-atmosphere and surface IRFs calculated by the model in this way. More details on these simulations can be found in DallaSanta & Polvani (2022).

2.2. VolMIP simulations

To assess the robustness of results from the GISS model, we supplement the above analysis with a multi-model evaluation of simulations from the Volcanic Forcing Model Intercomparison Project (VolMIP) (Zanchettin et al., 2016). In particular, we analyze all available model output for the central VolMIP experiment, *volc-pinatubo*, which simulates the response to an idealized Pinatubo-like eruption. In that experiment, volcanic aerosol radiative forcings were prescribed into the models using the CMIP6 reconstruction of the actual event (Thomason et al., 2016). The five models we analyze are CanESM5, GISS ModelE2.1, MIROC-ES2L, MPI-ESM1.2-LR, UKESM1. We use 25 simulations of each model, a number stipulated in the VolMIP protocol. We use output for the two-year period beginning with the eruption, as this was the largest number of full post-eruption years available from all models. Note that this is shorter than the four-year period we use our ModelE2.2 analysis, and that the GISS simulations in VolMIP are from a different model version (ModelE2.1) with fewer vertical levels (40) and a lower model top (0.01 hPa). Unlike our ModelE2.2 simulations, all VolMIP simulations have interactive SSTs, and hence fast and slow precipitation responses cannot be separately evaluated for the VolMIP models.

2.3 Radiative kernel analysis

We use radiative kernels to elucidate the mechanisms through which volcanic aerosols influence precipitation by altering radiative fluxes. In the radiative kernel method, simulated changes to a state variable are multiplied by kernels quantifying changes in radiative flux for a unit change in the variable at each location, altitude, and month-of-year (Soden et al., 2008). Temperature, water vapor, and surface albedo responses can be directly calculated with the kernels. To quantify the atmospheric radiative responses that drive precipitation change, we subtract kernels of surface responses from those representing top-of-atmosphere responses (Previdi, 2010).

We primarily use the CloudSat radiative kernels (Kramer et al., 2019), as they are based on satellite observations unlike older kernels that relied on global climate model output. To confirm that our key results are not kernel dependent, in our VolMIP analysis we additionally use kernels made with the GFDL (Soden et al., 2008) and ECHAM6 (Block & Mauritsen, 2013) models. In our analyses, we separate the atmospheric temperature response into two regions, above and below 200 hPa. We base this separation on the approximate boundary between aerosol-induced warming above and cooling below that level, to distinguish the impacts of these temperature responses. Cloud responses are not directly calculated by these kernels, yet can be estimated as a remainder. Since the VolMIP models did not output the aerosol IRF, we here treat the difference between the simulated radiative flux anomalies and all kernel-derived responses as a combined 'aerosol forcing + cloud response'.

3. Results

3.1. Linking post-eruption precipitation reduction to the atmosphere's energy balance

We first examine post-eruption global precipitation reduction in our model, establish the extent to which it is associated with fast and slow responses, and verify that diabatic cooling is a useful indicator of the precipitation response to volcanic aerosols. We start by presenting the decline in global mean precipitation in the GISS ModelE2.2 simulations of a 20 Tg S eruption. As seen in Fig. 1a, within 3 months of the simulated eruptions, global mean precipitation is negative. This is true not only for the ensemble mean (solid black line), but for all ensemble members (gray area). This decline in global precipitation is sustained for several years in the ensemble mean, and for one and a half years in every ensemble member. The ensemble mean decline in precipitation over the 4 post-eruption years amounts to a 2% reduction, with 4% reduction during the month of maximum response, nearly one year after the eruption.

We next consider the precipitation in the fixed SST ensemble in order to disentangle the roles of the fast and slow responses. Both the fast precipitation response (dashed black line) and slow response (difference between solid and dashed black lines) are revealed to be important. However, the fast response on average lasts slightly less than two years, due to its dependence on the presence of volcanic aerosols. In contrast, the slow response – which becomes the largest precipitation driver after the first six months – lasts for several years: this is due to the far longer

time scale for the ocean to equilibrate compared to the atmosphere. In the next section we will examine the fast and slow responses in more depth.

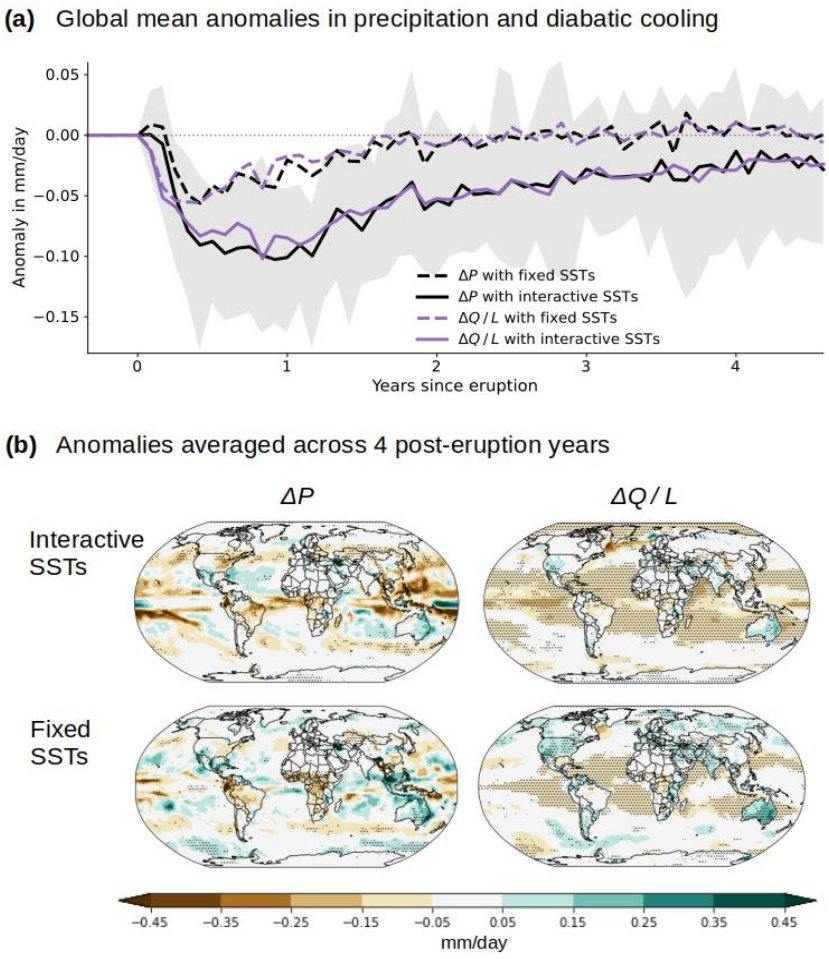

Figure 1 | Post-eruption global precipitation reduction in GISS ModelE2.2 experiments. (a) Time series of precipitation anomalies averaged across the ensemble of 20 Tg S eruptions and **(b)** maps of anomalies averaged over the four years following the eruption. In (a) precipitation anomalies are shown along with the concurrent diabatic cooling (divided by L to be in precipitation units). Shading in (a) denotes the full spread across the interactive SST ensemble, while stippling in (b) denotes agreement in sign among at least 80% of members in the presented ensemble.

We now demonstrate that post-eruption precipitation anomalies closely balance diabatic cooling from the sum of radiative and sensible heat flux anomalies, which we convert into precipitation-equivalent units ($\Delta Q / L$) and plot in Fig. 1a. Comparing the purple $\Delta Q / L$ lines of Fig. 1a to the black ΔP lines, it is clear that this diabatic cooling closely approximates post-eruption precipitation anomalies on a global scale. While this is well-known in simulation experiments with sustained forcings (Dagan et al., 2021; O'Gorman et al., 2012), the relationship has not been previously shown to hold with transient forcings such as tropical eruptions. The precipitation

response's lag behind diabatic cooling in the first post-eruption months (see the two solid lines) reflects the slow time scale on which the atmosphere fully adjusts to a stratospheric forcing, but no substantial difference persists after the first year. We interpret this as reflecting the shorter time-scale of the SST-mediated response that becomes dominant over time: compared to the stratosphere, the surface is more readily coupled to precipitation in the troposphere. These results confirm that diabatic cooling is a useful indicator of post-eruption precipitation response.

On regional scales (Fig. 1b), one sees a weaker relationship between diabatic cooling and precipitation than on global average, as energy transport ΔH also becomes important. We note for instance that ΔH drives a fast response of reduced precipitation over land areas, possibly due to land surface cooling inhibiting convection-driven circulations (Khodri et al., 2017). Contrasting the top and bottom panels in Fig. 1b, we see that ΔH leads to sharper differences in precipitation response across regions, and a larger spread across ensemble members. We emphasize that, even for such relatively large eruptions, the precipitation response lacks robustness across ensemble members nearly everywhere. This is evident in the lack of locations with least 80% of agreement in sign among ensemble members (stippling in the ΔP maps of Fig. 1b). Nonetheless, diabatic cooling controls precipitation anomalies over large spatial scales, as is especially apparent in the interactive SST simulations. Diabatic cooling, therefore, provides the baseline over which post-eruption precipitation anomalies due to energy transport occur, and is at many locations robust across eruption realizations. While we here focus primarily on global precipitation, impacts of diabatic cooling are thus important for the regional response as well.

3.2. Mechanisms of post-eruption precipitation response

We now decompose the diabatic cooling response to eruptions in ModelE2.2 in order to deduce the underlying mechanisms driving global precipitation reduction. In the left panel of Fig. 2a, we plot the four components of the energy balance as grouped by the curly brackets below Eqn. 2, but with the terms reordered to highlight the causality sequence, from the initial aerosol IRF to the resulting precipitation response. The volcanic aerosol forcing adds energy directly into the atmosphere via absorption of longwave radiation. This and aerosol-induced solar reflection drive rapid adjustments and SST-mediated responses in both radiative and sensible heat, along with latent heat responses from the resulting precipitation changes. These four terms in the left panel closely balance each other, summing to a negligible -0.006 W/m^2. Note that the volcanic aerosol forcing and SST-mediated diabatic cooling both bring energy into the atmosphere, whereas the rapid adjustments and precipitation (latent heat) reduction remove energy to restore equilibrium.

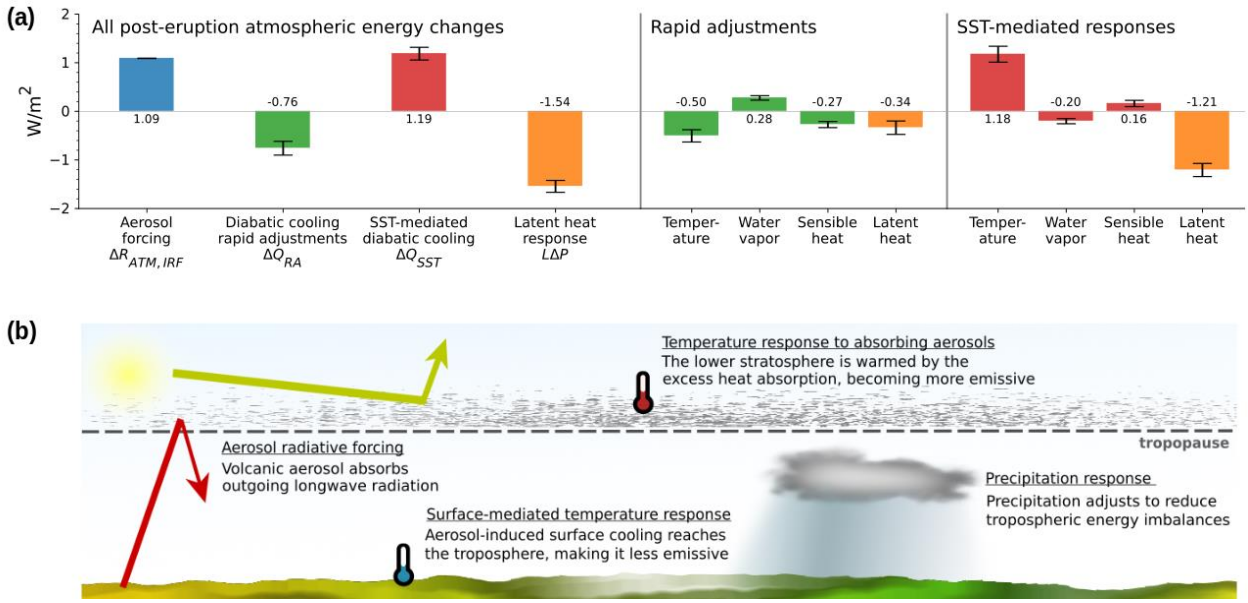

Figure 2 | Atmospheric energetic perturbations after a volcanic eruption in GISS ModelE2.2 experiments. In (a) each bar shows the ensemble mean quantified over the four-year period beginning with the month of the eruption, while uncertainties denote ±1 standard deviation among ensemble members. In (b) we visualize the dominant perturbations.

In the middle and right panels of Fig. 2a, we show the dominant terms in the rapid adjustments and SST-mediated responses. In those panels, the radiative term ΔR_{ATM} is decomposed using the CloudSat radiative kernels, as described in Methods, though we show only the temperature and water vapor responses that dominate the signal. The water vapor and sensible heat terms closely cancel each other, and also cancel when combining the rapid adjustment and SST-mediated responses for each. We will hence focus primarily on the aerosol forcing, the temperature rapid adjustment, and the SST-mediated temperature response as key to understanding the global precipitation response to volcanic aerosols.

Before focusing on those in depth, however, we note the role of two other energy terms. First, sensible heat flux rapid adjustments reduce energy in the atmosphere over land while adding energy over oceans (see Fig. S1). Though our focus is global, this partly explains why most diabatic cooling and precipitation reduction occurs over oceans in Fig. 1b. Our finding here resembles the land-ocean contrasts identified in the sensible heat responses to greenhouse gases and tropospheric aerosols (Myhre et al., 2018). Second, the fixed SST simulations reveal -0.26 W/m^2 (not shown) of rapid adjustments not attributed by the kernels to temperature, water vapor, or surface albedo adjustments. This may reflect cloud responses similar to those identified in assessments of the precipitation response to CO_2 (Kamae et al., 2015), though we lack sufficient model output (particularly clear-sky IRFs) to isolate cloud responses from non-cloud responses.

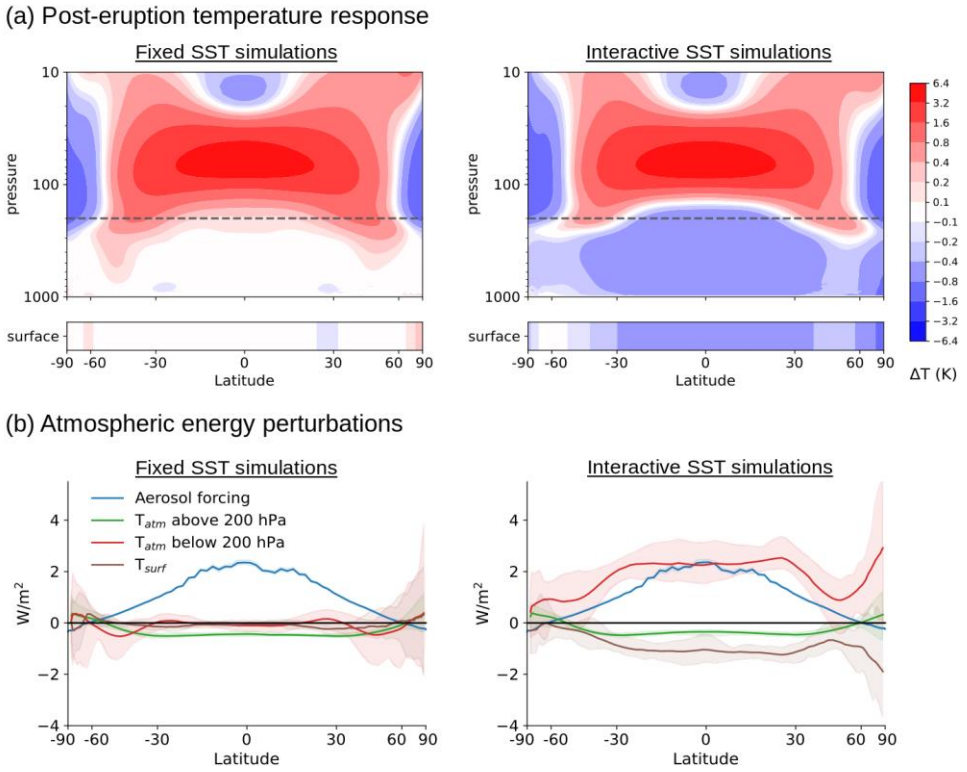

Figure 3 | Post-eruption (a) temperature changes and (b) the associated kernel-derived atmospheric energy responses. Results shown are ensemble means averaged over the 4 post-eruption years. Shading in (b) denotes the full spread among ensemble members, and solid lines represent ensemble means.

We now identify the mechanisms driving the precipitation fast response. Absorption of outgoing longwave radiation by volcanic aerosols adds a flux of energy into the atmosphere that dominates the aerosol forcing shown in Fig. 2a. This flux is reduced 35% compared to the longwave IRF alone (not shown) by the aerosol layer simultaneously reflecting sunlight away from underlying shortwave absorbers (e.g. water vapor and black carbon). Further, because the added energy flux is colocated with the aerosols in the stratosphere, it cannot readily be balanced by latent heat response in the underlying troposphere. Instead, the surplus energy causes the air surrounding the aerosol layer to warm, as shown in the left panel of Fig. 3a. This in turn enhances the emissivity of the atmosphere via Planck's law, primarily above 200 hPa, which offsets the excess energy flux. This emissivity response is shown as the green line in Fig. 3b, and is the dominant contributor to both the temperature rapid adjustment and total rapid adjustments, excluding latent heat (see Fig. 2a). Hence, the total stratospheric energy flux imbalance is smaller than the instantaneous aerosol forcing. This stratospheric diabatic cooling drives a global precipitation reduction that restores energetic balance (see the latent heat rapid adjustment in Fig. 2a, equal to the four-year average of the dashed black line in Fig. 1 scaled by L). We do not here rigorously deduce the pathway by which precipitation responds to an energetic imbalance centered in the overlying stratosphere. However, we expect this stems from increased flux of

longwave radiation from stratosphere-to-troposphere. This would thermodynamically inhibit precipitation when the excess longwave flux is absorbed by clouds or co-located greenhouse gases.

We next identify the mechanisms driving the slow precipitation response which, we recall, is an indirect response resulting from the reflection of incoming sunlight away from Earth's surface by the volcanic aerosol layer. The reflection of sunlight primarily affects the atmospheric energy budget by cooling the surface due to it being less insolated than before the eruption. Because tropospheric temperature is largely controlled by the underlying surface, the surface cooling in turn cools the troposphere (see the right panel of Fig. 3a). The tropospheric temperature anomaly is overall stronger than at surface, as occurs in response to greenhouse gases (Manabe & Wetherald, 1975; Santer et al., 2005), and also because of this the decreased emissivity of the atmosphere due to tropospheric cooling overpowers the decreased emissivity of the surface into the troposphere due to surface cooling (compare red and brown lines, respectively, in the right panel of Fig. 3b). Hence the SST-mediated temperature response overall adds energy to the troposphere, which drives a closely balancing global precipitation reduction (compare SST-mediated temperature and latent heat responses in Fig. 2a). Hence, much of the global precipitation reduction over the assessed 4-year period is an indirect effect of aerosol-induced surface cooling rather than a direct effect of the aerosol's radiative influence on the atmospheric energy balance. This is the key result of our paper. The diagram in Fig. 2b illustrates the four dominant global atmospheric energy terms discussed above, and their physical meaning.

3.4 Model spread in post-eruption atmospheric energy budget responses

We next analyze the VolMIP models, to confirm that the identified mechanisms leading to post-eruption precipitation response are robust across climate models, and also are robust across radiative kernels. Our results are presented in Fig. 4, where different colors show different models, and different symbols show different kernels. We note some methodological differences from the previous section. First, the VolMIP output analyzed here is for the 7-9 Tg S injection from Mt. Pinatubo, not a 20 Tg S idealized eruption. Second, we cannot separate rapid adjustments from SST-mediated responses here, because all VolMIP simulations use interactive SSTs.

Nonetheless, as one can see in Fig. 4, the VolMIP models confirm the results of the previous section. First, all combinations of models and kernels show that temperature anomalies above 200 hPa remove energy from the atmosphere, with responses elsewhere (atmosphere below 200 hPa + surface) in sum adding energy. Second, the VolMIP models show that water vapor, surface albedo, and sensible heat responses are all too minor to substantially influence global precipitation change. Third, the VolMIP models confirm that combining all latent, sensible, and radiative flux terms, the energy imbalance is minimal, validating our methodology.

Unfortunately, not enough output is provided by VolMIP to separate aerosol IRFs from cloud responses, yet we anticipate that the cloud responses dominate the model spread. Our rationale for expecting the IRF's influence to be robust is that all the models prescribe the same volcanic

aerosol scenario in VolMIP, and models generally tend to use identical volcanic aerosol optical properties (Palmer & Williams, 1975). Further study is needed to determine the influence of cloud responses on post-eruption precipitation response and its intermodel spread.

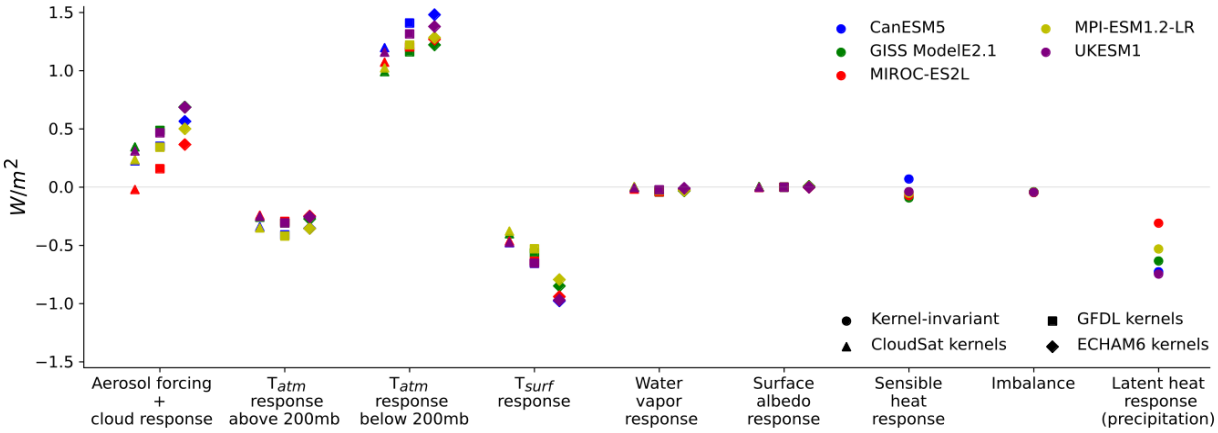

Figure 4 | Post-eruption intermodel spread across VolMIP, for ensemble means of five climate models simulating a Pinatubo-like eruption. We repeat this analysis using three sets of radiative kernels. Each color represents a different model, while each symbol represents a different kernels.

4. Conclusions

We have shown that global post-eruption precipitation reduction primarily stems from tropospheric cooling due to volcanic aerosols blocking incoming sunlight. As the assessed simulations revealed, this primary mechanism is mediated by cooler post-eruption SSTs. Absorption of outgoing longwave radiation by volcanic aerosols further reduces precipitation. This additional precipitation response is a rapid adjustment and dominates the precipitation decline in the first few post-eruption months, before the SST-mediated precipitation response overpowers it. These mechanisms are robust across climate models and radiative kernels.

Our analysis has identified and quantified the mechanisms linking volcanic aerosols to precipitation anomalies by harnessing the atmosphere's energy budget. This framework could prove useful for future evaluations of volcanic precipitation response. Furthermore, while we focused our evaluation on the global response to volcanic aerosols, the regional precipitation response to volcanism remains poorly studied outside of a few monsoon regions (Liu et al., 2016; Zhuo et al., 2020). It also remains to be seen how the mechanisms driving post-eruption precipitation reduction vary with eruption magnitude.

Acknowledgments

The authors thank Kevin DallaSanta for clarifications on the GISS ModelE2.2 simulations, which he had generated for a previous study. We also thank Dana Raiter and Ryan Kramer for useful discussions. This work was funded by the US National Science Foundation through award 1914569 to Columbia University.

Open Data

ModelE source code is available at https://www.giss.nasa.gov/tools/modelE/, and simulation output used here is on a Zenodo archive at https://doi.org/10.5281/zenodo.10407931. VolMIP data is available online at the CMIP6 repository, https://esgf-node.llnl.gov/projects/cmip6/.

References

Adler, R. F., Sapiano, M. R. P., Huffman, G. J., Wang, J.-J., Gu, G., Bolvin, D., et al. (2018). The Global Precipitation Climatology Project (GPCP) Monthly Analysis (New Version 2.3) and a Review of 2017 Global Precipitation. *Atmosphere*, *9*(4), 138. https://doi.org/10.3390/atmos9040138

Andrews, T., Forster, P. M., Boucher, O., Bellouin, N., & Jones, A. (2010). Precipitation, radiative forcing and global temperature change. *Geophysical Research Letters*, *37*(14). https://doi.org/10.1029/2010GL043991

Block, K., & Mauritsen, T. (2013). Forcing and feedback in the MPI-ESM-LR coupled model under abruptly quadrupled CO2. *Journal of Advances in Modeling Earth Systems*, *5*(4), 676–691. https://doi.org/10.1002/jame.20041

Dagan, G., & Stier, P. (2020). Constraint on precipitation response to climate change by combination of atmospheric energy and water budgets. *Npj Climate and Atmospheric Science*, *3*(1), 1–5. https://doi.org/10.1038/s41612-020-00137-8

Dagan, G., Stier, P., & Watson-Parris, D. (2021). An Energetic View on the Geographical Dependence of the Fast Aerosol Radiative Effects on Precipitation. *Journal of Geophysical Research: Atmospheres*, *126*(9), e2020JD033045. https://doi.org/10.1029/2020JD033045

DallaSanta, K., & Polvani, L. M. (2022). Volcanic stratospheric injections up to 160 Tg(S) yield a Eurasian winter warming indistinguishable from internal variability. *Atmospheric Chemistry and Physics Discussions*, 1–31. https://doi.org/10.5194/acp-2022-58

Gillett, N. P., Weaver, A. J., Zwiers, F. W., & Wehner, M. F. (2004). Detection of volcanic influence on global precipitation. *Geophysical Research Letters*, *31*(12). https://doi.org/10.1029/2004GL020044

Iles, C. E., & Hegerl, G. C. (2014). The global precipitation response to volcanic eruptions in the CMIP5 models. *Environmental Research Letters*, *9*(10), 104012. https://doi.org/10.1088/1748-9326/9/10/104012

Kamae, Y., Watanabe, M., Ogura, T., Yoshimori, M., & Shiogama, H. (2015). Rapid Adjustments of Cloud and Hydrological Cycle to Increasing CO2: a Review. *Current Climate Change Reports*, *1*(2), 103–113. https://doi.org/10.1007/s40641-015-0007-5

Khodri, M., Izumo, T., Vialard, J., Janicot, S., Cassou, C., Lengaigne, M., et al. (2017). Tropical explosive volcanic eruptions can trigger El Niño by cooling tropical Africa. *Nature Communications*, *8*(1), 778. https://doi.org/10.1038/s41467-017-00755-6

Kramer, R. J., Matus, A. V., Soden, B. J., & L'Ecuyer, T. S. (2019). Observation-Based Radiative Kernels From CloudSat/CALIPSO. *Journal of Geophysical Research: Atmospheres*, *124*(10), 5431–5444. https://doi.org/10.1029/2018JD029021

Liu, F., Chai, J., Wang, B., Liu, J., Zhang, X., & Wang, Z. (2016). Global monsoon precipitation responses to large volcanic eruptions. *Scientific Reports*, *6*(1), 24331. https://doi.org/10.1038/srep24331

Manabe, S., & Wetherald, R. T. (1975). The Effects of Doubling the CO2 Concentration on the climate of a General Circulation Model. *Journal of the Atmospheric Sciences*, *32*(1), 3–15. https://doi.org/10.1175/1520-0469(1975)032<0003:TEODTC>2.0.CO;2

Myhre, G., Samset, B. H., Hodnebrog, Ø., Andrews, T., Boucher, O., Faluvegi, G., et al. (2018). Sensible heat has significantly affected the global hydrological cycle over the historical period. *Nature Communications*, *9*(1), 1922. https://doi.org/10.1038/s41467-018-04307-4

O'Gorman, P. A., Allan, R. P., Byrne, M. P., & Previdi, M. (2012). Energetic Constraints on Precipitation Under Climate Change. *Surveys in Geophysics*, *33*(3), 585–608. https://doi.org/10.1007/s10712-011-9159-6

Orbe, C., Rind, D., Jonas, J., Nazarenko, L., Faluvegi, G., Murray, L. T., et al. (2020). GISS Model E2.2: A Climate Model Optimized for the Middle Atmosphere—2. Validation of Large-Scale Transport and Evaluation of Climate Response. *Journal of Geophysical Research: Atmospheres*, *125*(24), e2020JD033151. https://doi.org/10.1029/2020JD033151

Palmer, K. F., & Williams, D. (1975). Optical Constants of Sulfuric Acid; Application to the Clouds of Venus? *Applied Optics*, *14*(1), 208–219. https://doi.org/10.1364/AO.14.000208

Previdi, M. (2010). Radiative feedbacks on global precipitation. *Environmental Research Letters*, *5*(2), 025211. https://doi.org/10.1088/1748-9326/5/2/025211

Proctor, J., Hsiang, S., Burney, J., Burke, M., & Schlenker, W. (2018). Estimating global agricultural effects of geoengineering using volcanic eruptions. *Nature*, *560*(7719), 480–483. https://doi.org/10.1038/s41586-018-0417-3

Robock, A., & Liu, Y. (1994). The Volcanic Signal in Goddard Institute for Space Studies Three-Dimensional Model Simulations. *Journal of Climate*, *7*(1), 44–55. https://doi.org/10.1175/1520-0442(1994)007<0044:TVSIGI>2.0.CO;2

Samset, B. H., Myhre, G., Forster, P. M., Hodnebrog, Ø., Andrews, T., Faluvegi, G., et al. (2016). Fast and slow precipitation responses to individual climate forcers: A PDRMIP multimodel study. *Geophysical Research Letters*, *43*(6), 2782–2791. https://doi.org/10.1002/2016GL068064

Santer, B. D., Wigley, T. M. L., Mears, C., Wentz, F. J., Klein, S. A., Seidel, D. J., et al. (2005). Amplification of surface temperature trends and variability in the tropical atmosphere. *Science (New York, N.Y.)*, *309*(5740), 1551–1556. https://doi.org/10.1126/science.1114867

Soden, B. J., Held, I. M., Colman, R., Shell, K. M., Kiehl, J. T., & Shields, C. A. (2008). Quantifying Climate Feedbacks Using Radiative Kernels. *Journal of Climate*, *21*(14), 3504–3520. https://doi.org/10.1175/2007JCLI2110.1

Thomason, Larry, Vernier, Jean-Paul, Bourassa, Adam, Arfeuille, Florian, Bingen, Christine, Peter, Thomas, & Luo, Beiping. (2016). Stratospheric Aerosol Data Set (SADS Version 2) Prospectus. Retrieved from https://www.wcrp-climate.org/images/modelling/WGCM/CMIP/CMIP6Forcings_StratosphericAerosolDataSet_InitialDescription_150131.pdf

Toohey, M., Stevens, B., Schmidt, H., & Timmreck, C. (2016). Easy Volcanic Aerosol (EVA v1.0): an idealized forcing generator for climate simulations. *Geoscientific Model Development*, *9*(11), 4049–4070. https://doi.org/10.5194/gmd-9-4049-2016

Trenberth, K. E., & Dai, A. (2007). Effects of Mount Pinatubo volcanic eruption on the hydrological cycle as an analog of geoengineering. *Geophysical Research Letters*, *34*(15). https://doi.org/10.1029/2007GL030524

Zanchettin, D., Khodri, M., Timmreck, C., Toohey, M., Schmidt, A., Gerber, E. P., et al. (2016). The Model Intercomparison Project on the climatic response to Volcanic forcing (VolMIP): experimental design and forcing input data for CMIP6. *Geoscientific Model Development*, *9*(8), 2701–2719. https://doi.org/10.5194/gmd-9-2701-2016

Zhuo, Z., Gao, C., Kirchner, I., & Cubasch, U. (2020). Impact of Volcanic Aerosols on the Hydrology of the Asian Monsoon and Westerlies-Dominated Subregions: Comparison of Proxy and Multimodel Ensemble Means. *Journal of Geophysical Research: Atmospheres*, *125*(18), e2020JD032831. https://doi.org/10.1029/2020JD032831